Dynamical analysis of a periodically forced chaotic chemical oscillator

Ramírez-Ávila, Gonzalo Marcelo; Kapitaniak, Tomasz; Gonze, Didier

Published in:
Chaos

DOI:
10.1063/5.0213913

Publication date:
2024

Document Version
Peer reviewed version

Chaos
An Interdisciplinary Journal
of Nonlinear Science

AIP Publishing

Dynamical analysis of a periodically forced chaotic chemical oscillator

Gonzalo Marcelo Ramírez-Ávila,[1,2,3,4,a)] Tomasz Kapitaniak,[2] and Didier Gonze[4]
[1)] *Namur Institute for Complex Systems (naXys), Université de Namur, Rue de Bruxelles 61, B-5000 Namur, Belgium*
[2)] *Division of Dynamics, Lodz University of Technology, Stefanowskiego 1/15, 90-924 Lodz, Poland*
[3)] *Instituto de Investigaciones Fisicas, and Planetario Max Schreier, Universidad Mayor de San Andres, Campus Universitario, C. 27 s/n Cota-Cota, 0000 La Paz, Bolivia*
[4)] *Unit of Theoretical Chronobiology, Université Libre de Bruxelles, CP231, Boulevard du Triomphe, 1050 Brussels, Belgium*

We present a comprehensive dynamical analysis of a chaotic chemical model referred to as the autocatalator, when subject to a periodic administration of one substrate. Our investigation encompasses the dynamical characterization of both unforced and forced systems utilizing isospikes and largest Lyapunov exponents-based parameter planes, bifurcation diagrams, and analysis of complex oscillations. Additionally, we present a phase diagram showing the effect of the period and amplitude of the forcing signal on the system's behavior. Furthermore, we show how the landscapes of parameter planes are altered in response to forcing application. This analysis contributes to a deeper understanding of the intricate dynamics induced by the periodic forcing of a chaotic system.

Keywords: Nonlinear dynamics, chaotic chemical reactions, forced systems

Periodic forcing of chemical and biological oscillators has been extensively studied, both analytically and numerically. However, the effect of periodic forcing on chaotic systems received much less attention. Here, we investigate this question through numerical simulations of a three-variable chaotic system, referred to as the autocatalator. The application of periodic forcing in this system unveils several interesting aspects, including the emergence of complex limit cycles. We characterize these behaviors as a function of the forcing signal's amplitude and period. Qualitative transformations in the dynamical landscapes of parameter planes are observed under forcing effects.

I. INTRODUCTION

Since the first experimental demonstrations of chaotic behavior in chemical systems such as the Belousov-Zhabotinskii (BZ) reaction[63] and the peroxidase-oxidase system[51], complex oscillations and chaotic dynamics have been reported in numerous models for chemical and biological systems. They originate from various mechanisms such as interlocked feedback loops, autocatalytic processes, coupled oscillators, and the influence of periodic external inputs, either independently or in combination[2,25,26,30,35,38,61,62,71]. While these phenomena represent a broad array of behaviors, their uncontrolled presence poses challenges both in natural contexts and practical applications, necessitating methods for their regulation or elimination. In the realm of chaos control, periodic forcing stands as a potential strategy to convert chaotic dynamics into more regular limit cycle oscillations. A deeper comprehension of the implications of periodic forcing on chaotic systems is needed. In this study, we performed a systematic numerical analysis of a prototypical chaotic chemical system to explore the effect of periodic forcing on chaotic dynamics.

In the 1990s, Showalter and colleagues described a three-variable chemical system unveiling a rich repertoire of behaviors including period doubling, chaos[53], and mixed-mode oscillations (MMOs)[54]. A bifurcation analysis revealed the emergence of branches of isolas of limit cycles and Devil's staircase structures when scrutinizing the firing number—a metric denoting the proportion of large peaks relative to the total number of peaks per period—as a function of a control kinetic parameter. The concept of isolas of limit cycles constitutes the basis of the analysis in terms of isospikes[17] that we use in this work. Kawczynski and colleagues introduced an alternative three-variable model, which qualitatively captures the phenomenon of mixed-mode oscillations (MMOs) observed in the Belousov-Zhabotinsky (BZ) reaction[41,57]. This model is not associated with a system of chemical reactions, but instead, it can be seen as an extension of the Fitzhugh-Nagumo model used in neurophysiology. Kalishin et al. (2002)[39] studied a detailed kinetic model for the BZ reaction and showed both experimentally and theoretically the emergence of a wide variety of oscillatory complex behavior, including MMOs, quasiperiodicity, and chaos as kinetic parameters are changed. Similar behaviors have been obtained by Ivanovic-Sasic et al. (2011)[36] using a detailed model for the Bray-Liebhafsky reaction. The emergence of chaotic oscillations was recently reported in an enzyme-catalyzed reaction, namely the peroxidase-oxidase reaction[50,52].

Chaos and complex oscillations have also been reported in various biological systems spanning diverse time scales[24,27]. Among the most important examples from the physiological viewpoint, we can mention those related to the experimental evidence and modeling of low dimensional chaos in cardiac tissue[7] and the electrical activity of the heart[56]. Similar approaches have been employed to describe the chaotic activities in the brain by experiments[11], models[1], or both[42]. Other examples include the experiments on metabolic reactions[48] and their modeling[9,30], genetic regulatory networks

[a)] gonzalo-marcelo.ramirezavila@unamur.be

models[43,46,70], the models[32,62] and experiments[66] of cell division cycle, and the models of circadian clocks[44,45,64]. Autonomous chaos may result from nonlinear interlocked feedback loops involving autocatalytic processes and/or coupled oscillatory mechanisms. The manifestation of chaos is inherent to systems undergoing periodic forcing[29,33,37]. The theory concerning Arnold's tongues (ATs) frequently finds application in delineating regions of entrainment as a function of the frequency and amplitude of the periodic input. Generally, escalating coupling strength manifests in a sequential progression featuring quasiperiodicity, limit cycle oscillations (entrainment), period-doubling, and, ultimately, chaotic dynamics[34].

Although chaos may have crucial constructive roles in biology as, for example, in the brain activity of the different stages of the sleep[4], in the heart rate variability as an indicator of the cardiovascular system's normal functioning[40], and in the fine-tuning of gene expression[33]; in several contexts, such complex dynamics need to be controlled and converted to regular oscillations. This is the case for instance in some types of epileptiform activity[3], and for the circadian clock to allow a proper adaptation to the light-dark cycle and to avoid sleep disorders[28,68]. Control of chaos refers to the stabilization of periodic orbits and thereby to the suppression of chaotic behavior. Approaches aimed at attaining this objective may rely on (delayed) feedback mechanisms[6,55] or input modulation techniques. For instance, Choe et al. (2005)[8] showed that the application of high-frequency periodic forcing to the Lorenz system could effectively suppress chaotic behavior. Stone (1992) successfully suppressed chaos within the Rössler system by employing periodic pulses whose frequencies closely aligned with the peaks of the attractor power spectrum [65].

The application of periodic forcing to chaotic systems has historically garnered less attention compared to its application to limit cycles[5,14,47]. In this study, we conducted numerical analyses to investigate the effects of periodic forcing on a three-variable chemical system previously shown to exhibit chaotic oscillations (Sect. II). Our choice is motivated by the fact that this kind of forcing might control several chemical and biological systems, especially in chronobiological-related situations. We first characterize various autonomous behaviors and show how they are distributed in the parameter space (Sect. III A). We then study the impact of periodic forcing on chaotic dynamics. We consider a sinusoidal forcing and discuss the effect of its amplitude and period on the resulting behavior. We also characterize the bifurcations induced by this periodic forcing and describe the alteration of the parameter plane's landscape in response to such a forcing (Sect. III B).

II. MODEL

As a minimal chemical model displaying chaos, we used the three-variable autocatalator, proposed by Peng et al. in 1990[53]. It describes the dynamics of the concentration of the compounds A, B, and C involved in the following reaction scheme:

$$\begin{aligned} \mathrm{P} &\xrightarrow{k_0} \mathrm{A} \\ \mathrm{P{+}C} &\xrightarrow{k_c} \mathrm{A{+}C} \\ \mathrm{A} &\xrightarrow{k_u} \mathrm{B} \\ \mathrm{A{+}2B} &\xrightarrow{k_1} \mathrm{3B} \\ \mathrm{B} &\xrightarrow{k_2} \mathrm{C} \\ \mathrm{C} &\xrightarrow{k_3} \mathrm{D} \quad . \end{aligned}$$

Utilizing the law of mass action, the kinetic equations governing this system can be expressed as follows:

$$\frac{\mathrm{d}A}{\mathrm{d}t} = k_0 P + k_c PC - k_u A - k_1 AB^2 \tag{1}$$

$$\frac{\mathrm{d}B}{\mathrm{d}t} = k_u A + k_1 AB^2 - k_2 B \tag{2}$$

$$\frac{\mathrm{d}C}{\mathrm{d}t} = k_2 B - k_3 C \quad . \tag{3}$$

We assume that P, the concentration of P, remains constant. The product D is an output, and its concentration D does not affect the kinetics of the reactions. The structure of the system is represented in Fig. 1. This schematic emphasizes the autocatalytic production of B and the positive feedback exerted by C on the reaction P $\rightarrow$ A. The interplay between these regulatory mechanisms allows the system to engender chaotic oscillations[53,54]. The default parameter values, under which autonomous chaos is observed, are as follows: $k_0 = 260$, $k_c = 1$, $k_u = 1$, $k_1 = 1$, $k_2 = 0.2 \times 10^3$, $k_3 = 0.5 \times 10^2$, and $P = 7.7$ (all values in arbitrary units).

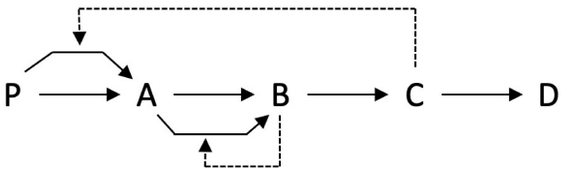

Figure 1. Scheme of the model. Dashed arrows denote regulatory interactions, including autocatalysis and positive feedback mechanisms.

We introduce a periodic sinusoidal forcing applied to the parameter P, the concentration of the input reactant P:

$$P \rightarrow P\left[1 + \frac{F}{2}\left(1 + \sin\frac{2\pi t}{T}\right)\right] \quad . \tag{4}$$

where F and T are, respectively, the amplitude and the period of the forcing. In this work,, we will discuss the impact of these two parameters on the system's behavior.

Numerical integration of Eqs. (1)–(3) are executed with a fourth-order Runge-Kutta method with a time step $h = 10^{-5}$. Unless stated otherwise, the transient time is set to 5×10^6 and the total integration time to 10^7. Parameter planes are generated with a 1024×1024 pixels resolution.

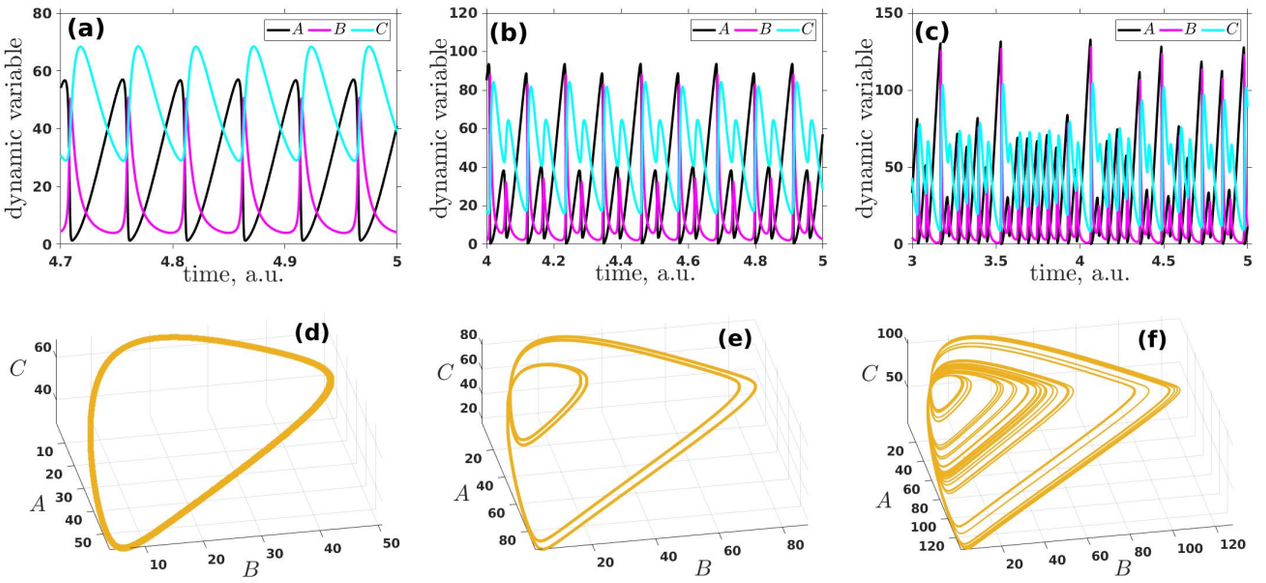

Figure 2. Time series for the dynamic variables A, B and C when the parameters are fixed to $k_0 = 260$, $k_c = k_u = k_1 = 1$, $k_2 = 200$, $k_3 = 50$, and P is chosen for leading the system to different dynamical regimes after a determined transient t_s. (a) $P = 7.83$, limit cycle-1, $t_s = 4.7$, (b) $P = 7.78$, limit cycle-4, $t_s = 4.0$, and (c) $P = 7.70$, chaos, $t_s = 3.0$. The corresponding attractors for the aforementioned scenarios are depicted in panels (d)–(f). In all cases, the initial conditions are set to $(A_0, B_0, C_0) = (1, 1, 1)$.

III. RESULTS

A. Unforced case

Despite its apparent simplicity, the model exhibits a vast dynamical richness depending on the parameter values. Figure 2 shows the time series and the corresponding attractors for different values of P (taken constant). Three distinct scenarios are illustrated: limit cycle-1 (Figs. 2(a) and (d)), limit cycle-4 (Figs. 2(b) and (e)), and chaotic attractor (Figs. 2(c) and (f)). The number accompanying the limit cycle indicates the number of isospikes per complete period. We can also note that the amplitude and period of the oscillations depend on P. The attractors illustrated in Fig. 2(d)–(e) exhibit similar overall shapes but also reflect disparities in the amplitudes of the oscillations. These amplitudes tend to increase with the complexity of the oscillatory behavior. Consequently, a limit cycle-1 occupies a smaller phase volume compared to a limit cycle-4 and significantly less than that of a chaotic attractor.

In this study, we conduct an exhaustive dynamical analysis encompassing both unforced (autonomous) and forced (nonautonomous) systems. Our analytical approach relies on various tools, including time series and attractors analysis, bifurcation diagrams (BDs), and exploration of parameter planes (PPs) based on the largest Lyapunov exponents (LLEs) or isospikes. Isospikes and LLEs serve as valuable instruments in the characterization of dynamic chemical systems, as evidenced in diverse contexts such as the Belousov-Zhabotinsky reaction[12,16,17,20], triple-pathway electro-oxidation of formic acid on platinum[15], peroxidase-oxidase reaction models[21,22,50,52], and theoretical reaction systems[18,21]. From the time series generated by the numerical integration of Eqs. (1)–(3), we compute the Lyapunov spectrum using the method of Wolf et al.[67] from which the LLE is selected to construct the PP. Concerning the computation of isospikes, they are also obtained from the time series by counting the number of spikes (maxima) contained in each oscillatory cycle when the dynamical behavior is nonchaotic.

Next, we perform a systematic analysis with the intent of giving an exhaustive overview of the dynamics of the autocatalator. One of the methods to extract meaningful information about the dynamical system is to screen the parameter space. In this study, we concentrate on chaotic regions in the (k_u,P) plane (Fig. 3). Each row of Fig. 3 presents a dynamic characterization of the system in terms of isospikes (first row), largest Lyapunov exponents (LLEs) (second row), and bifurcation diagrams (BDs) (third row). In the isospikes-PP, colors are associated with distinct periodicities based on the number of maxima within each period of the oscillation (isospikes), while black indicates chaotic behavior. The color code shown below the first row shows the number of isospikes from 1 to 34, and situations with 35 or more isospikes are represented by dark gray. Figure 3(a) exhibits regions characterized by a monotonically increasing number of isospikes (3, 4, 5, 6, 7, ...) form distinct patterns resembling petals. These regions predominantly exhibit periodic behavior, interspersed with smaller chaotic regions. Intriguingly, these chaotic interstices diminish in size as the number of isospikes increases.

Two distinct chaotic interstices were selected to better visualize the dynamic structure within each region, which are

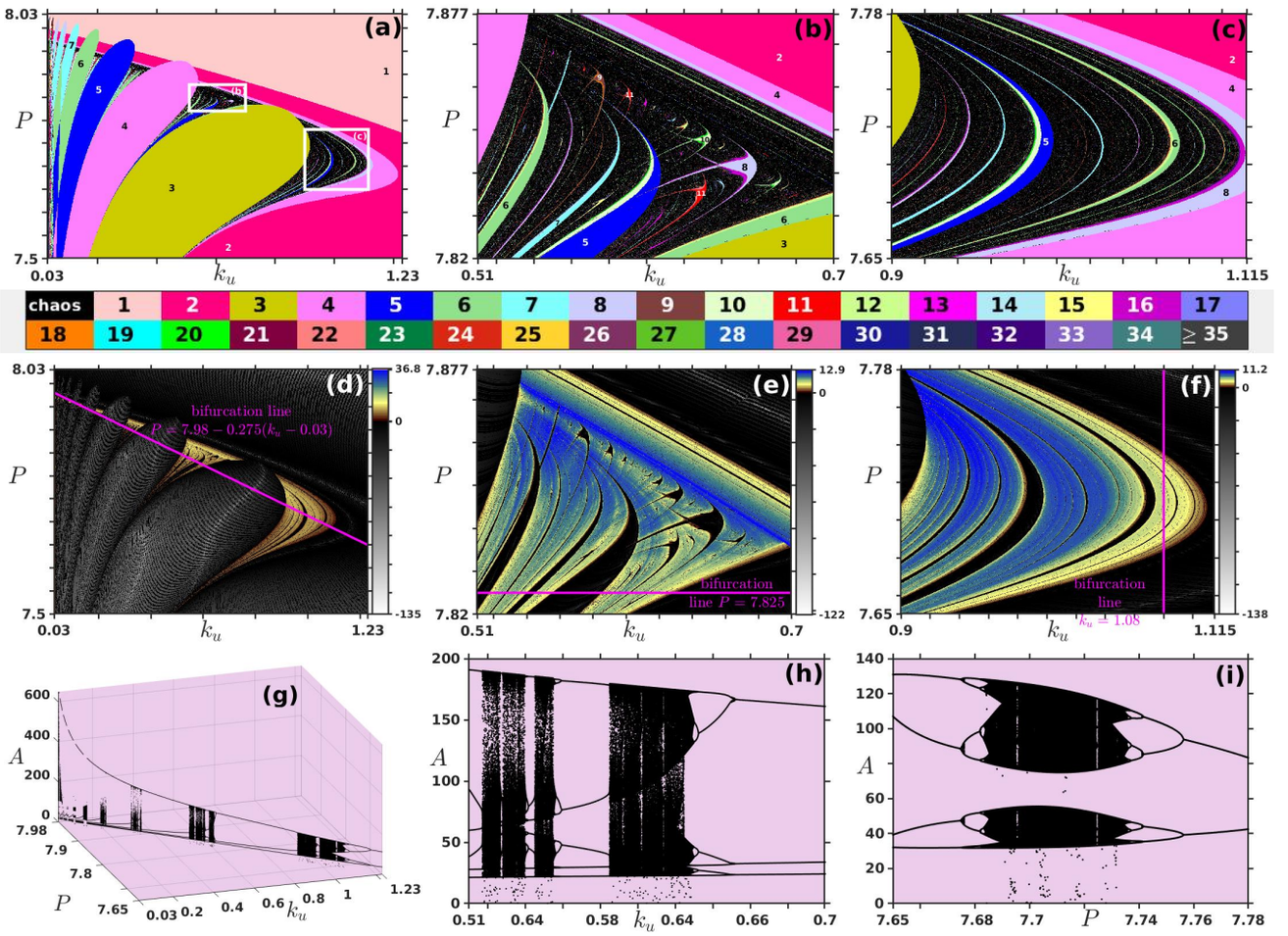

Figure 3. Parameter space analysis for the non-forced autocatalator. (a) Parameter plane (PP) showing the regions of chaotic regimes when varying k_u and P. Regions outlined with rectangles are enlarged in panels (b) and (c). The color scale at the bottom indicates the number of isospikes per time period. Regular oscillatory behavior and chaotic dynamics are represented in color and black, respectively. Panels (d)–(f) display the same PPs as those in the top row but represented in terms of the largest Lyapunov exponents (LLEs), with corresponding values given by the color bar positioned to the right of each panel. (g)–(i) Bifurcation diagrams (BDs) corresponding to the straight magenta line drawn in panels (d)–(f), with (g) $P = 7.98 - 0.275(k_u - 0.33)$, (h) $P = 7.825$, and (i) $k_u = 1.08$. All parameter values and initial conditions are as in Fig. 2.

zoomed in Figs. 3(b)–(c). Figure 3(b) illustrates the chaotic predominant interstice situated between the "petals" associated with three and four isospikes. The upper and lower right boundaries of the chaotic region in Figs. 3(b)–(c) show a period-doubling route to chaos, as reflected by the varying number of isospikes. Conversely, the contours in the upper-left quadrants in Figs. 3(b)–(c) exhibit no discernible period-doubling behavior. This observation suggests that the strong convex portion of each "petal" contouring the chaotic region experiences an abrupt transition to chaos, whereas if the contour of the "petal" locally displays a weak convexity, there is a period-doubling route to chaos. In other words, while the upper right portion of a "petal" maintains a consistent number of isospikes, the upper left part displays a period-doubling route to chaos. Within the chaotic interstice depicted in Fig. 3(b), intricate filiform structures are discerned, characterized by a predominant number of isospikes ranging from five to six. Sequences of "shrimps" exhibiting an increasing number of isospikes and converging toward accumulation points are observed in the central region of Fig. 3(b). These sequences are distinguished by increments of 8, 10, 12, ... and 9, 11, 13, ..., respectively. Similarly, falciform structures appear in the chaotic interstice presented in Fig. 3(c), primarily characterized by a prevailing number of isospikes ranging from five to six. We observe that all the above-mentioned structures inside the chaotic interstices display a period-doubling route to chaos in their concave regions; thus corroborating our previous observation that convexity favors an abrupt passage to chaos.

The PPs represented in terms of the LLEs are depicted in Figs. 3(d)–(f), where black and white regions denote regular or periodic behavior of the system, respectively, while colored regions stand for chaotic behavior. When comparing the

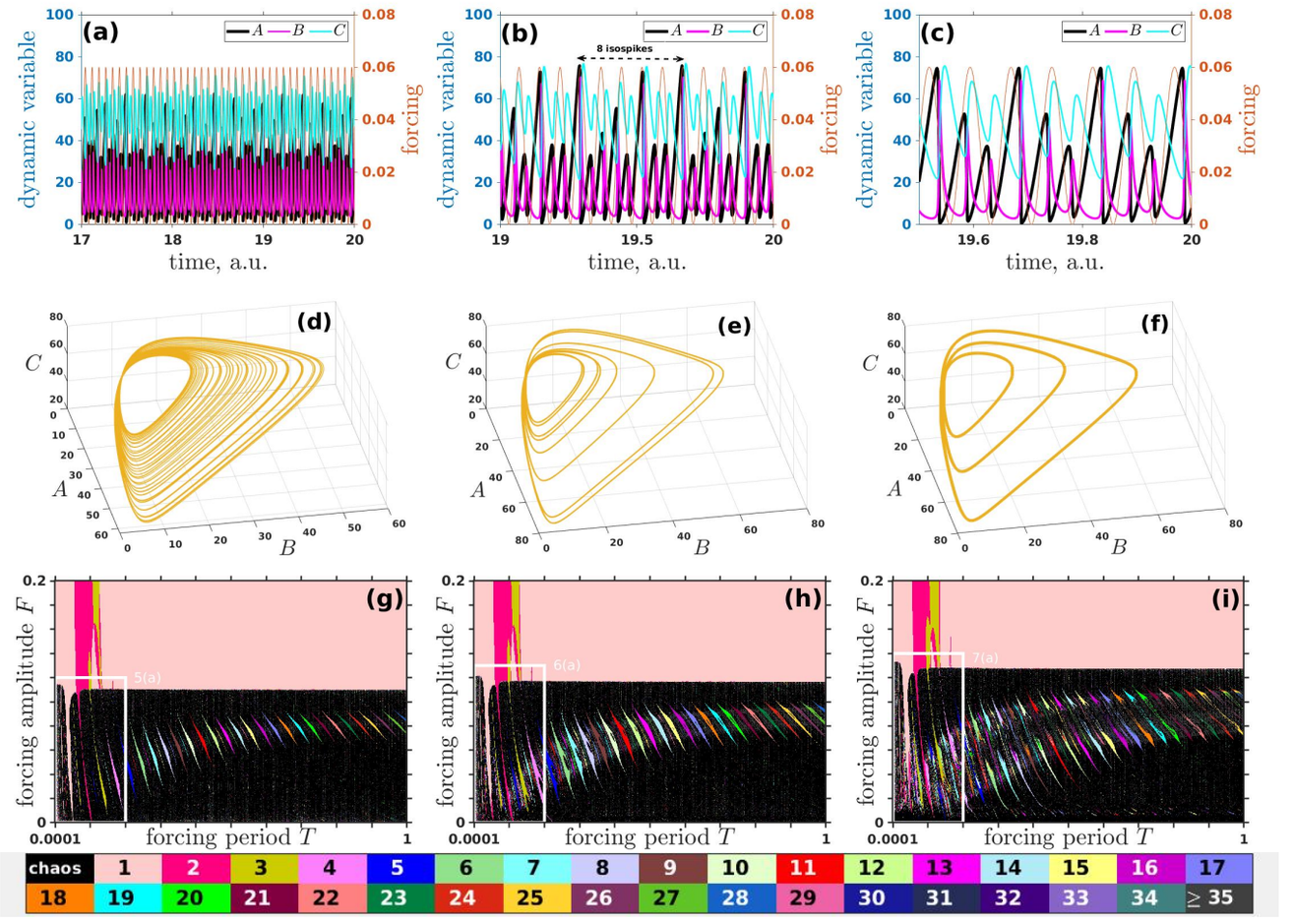

Figure 4. Effect of periodic forcing on the autocatalator. (a)–(c) Time series for the dynamic variables A, B and C and the corresponding attractors (d)–(f) when a sinusoidal forcing with period $T = 0.075$ and amplitude $F = 0.03$ is applied. (a) and (d) $P = 7.83$, the unforced limit cycle-1 (Fig. 2(d)) becomes a chaotic attractor. (b) and (e) $P = 7.78$, the unforced limit cycle-4 (Fig. 2(e)) becomes a limit cycle-8. (c) and (f) $P = 7.70$, the unforced chaotic attractor (Fig. 2(f)) becomes a limit cycle-3. (g)–(i) Parameter planes showing the effect of the period T and amplitude F for each scenario, based on the variable A. Rectangular regions within each plane (g)–(i) are enlarged in Figs. 5(a), 6(a), and 7(a), respectively. All parameter values and initial conditions are as in Fig. 2.

diagrams in the first and second rows, it is evident that the information is qualitatively the same, which allows us to use any of them. It is interesting to notice that the "petal" structures in Fig. 3(a) look like "fingerprints" in Fig. 3(d). It is noteworthy to mention that the white stripes with the lowest LE values are related to superstable orbits as those found in maps[19]. In order to have a deeper insight into the system's dynamics, we compute some BDs corresponding to a specific situation in each of the three cases. Thus, in Fig. 3(d), it is represented in magenta the bifurcation line for which the BD is shown in Fig. 3(g). The chaotic regions shrink with increasing P (decreasing k_u). Conversely, amplitude oscillations enlarge with P. In Figs. 3(e)–(f), the bifurcation lines correspond to a horizontal and a vertical line given by $P = 7.825$ and $k_u = 1.08$ respectively whose BDs are represented in Figs. 3(h)–(i). The most common bifurcation scenario is period doubling. This comprehensive analysis underscores the rich dynamical behavior exhibited by the system. We cannot exclude situations where multiple attractors coexist. When computing the basin of attraction for some values of P corresponding to regular behavior, we observe a possible coexistence of limit cycles 8 and 16 (not shown). A systematic screening of the initial conditions and an in-depth characterization of possibly distinct, coexisting attractors is however out of the scope of the present paper.

B. Forced case

To investigate the impact of forcing on the system, we implemented the sinusoidal forcing method outlined in Sect. II and defined by Eq. (4). Figure 4 serves as an initial exploration into the influence of forcing on the system. We examine the three scenarios depicted in Fig. 2 where we applied

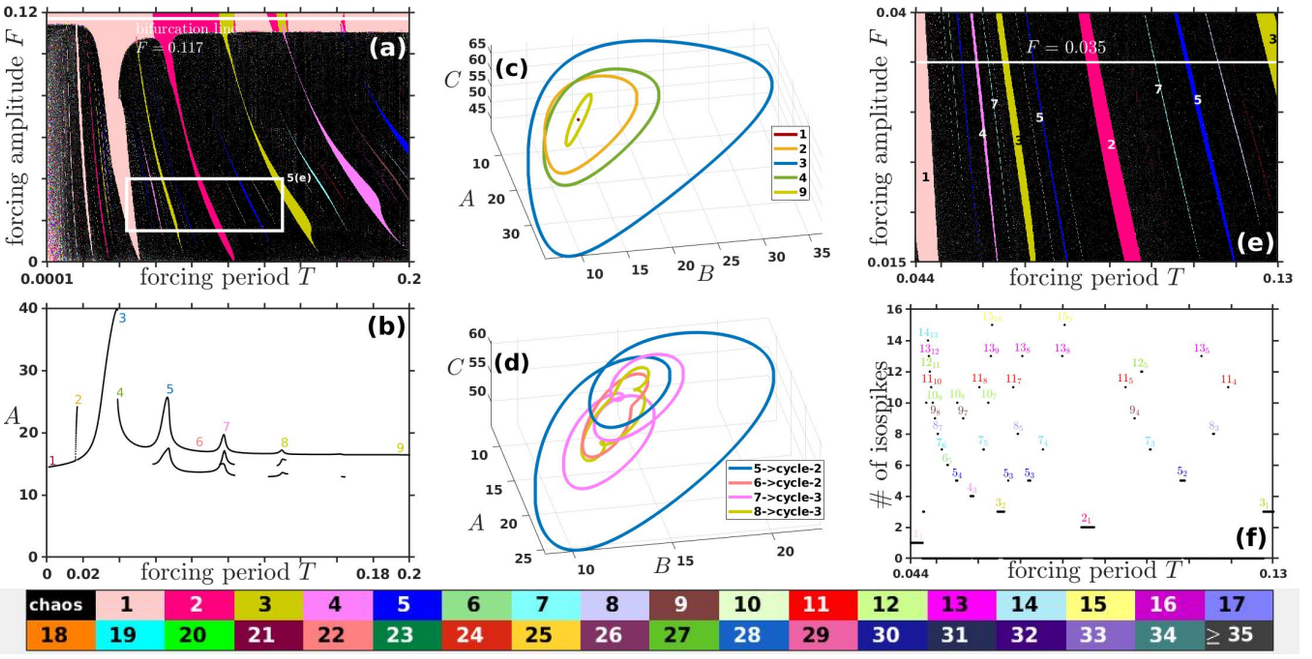

Figure 5. Analysis of the forcing regime when $P = 7.83$. **First column:** (a) Forcing phase diagram depicting F vs T for the variable A, corresponding to the magnified rectangular region of Fig. 4(g). (b) Bifurcation diagram reporting the dynamical variable A maxima as a function of the forcing period T for $F = 0.117$ (white line shown in panel (a)). **Second column:** The stable manifold for the marked points 1–9 of the bifurcation diagram are plotted in (c) for the limit cycle-1 (points 1–4 and 9), and (d) for the limit cycle-2 (points 5 and 6), and limit cycle-3 (points 7 and 8). **Third column:** (e) Magnification of the box on (a) showing the isospikes-adding behavior of the Arnold's tongues (ATs). (f) Plot of the number of isospikes as a function of the forcing period T throughout the line $F = 0.035$ of (e) showing a kind of devil's staircase pattern. The color bar provides information on the number of isospikes within the ATs depicted in (a) and (e).

a sinusoidal forcing with a period $T = 0.075$ and amplitude $F = 0.03$. Figure 4 illustrates the resulting time series (first row) and the corresponding attractors (second row). When the forcing is applied to the system with $P = 7.83$, the dynamic behavior transitions from limit cycle-1 to chaos (Figs. 4(a) and (d)). When applying the forcing to the system with $P = 7.78$ (limit cycle-4 state), the system maintains its regular behavior, acquiring a dynamic characterized by a limit cycle-8 (Figs. 4(b) and (e)). Finally, when the forcing is applied to the system with $P = 7.70$ (initially an unforced chaotic attractor), the system's behavior transforms into a limit cycle-3 (Figs. 4(c) and (f)).

A comprehensive examination of the dynamical effects induced by the forcing is presented in the third row of Fig. 4, featuring the forcing phase diagrams (FPDs). These diagrams depict the system's dynamic behavior in the F vs. T plane for specific regimes of the unforced system. Thus, Figs. 4(g)–(i) correspond to the FPDs of a limit cycle-1, a limit cycle-4, and a chaotic attractor, respectively. Several similarities and differences among the FPDs are noticeable. First, for small period values, a predominant region of limit cycle-1, referred to as the main Arnold's tongue (AT), is present in all cases, which aligns with the sinusoidal nature of the forcing signal, inherently inducing a limit cycle-1 response. We also note the presence of a threshold for the forcing amplitude above which entrainment of the system by the forcing signal is observed. Furthermore, sequences of AT-like structures are observed as the period increases and are associated with increasingly complex oscillatory behavior (i.e., with a greater number of isospikes per oscillation cycle). The shape and breadth of the ATs differ among cases, expanding when the forcing acts upon the system with chaotic unforced behavior, as shown in Fig. 4(i). The ATs generally exhibit monochromatic patterns, indicating oscillations with a consistent number of isospikes within each tongue. However, distinctions between the ATs of Figs. 4(g) and (h) emerge; particularly, Fig. 4(h) displays a peculiar hole-like structure reminiscent of ring structures[59] and the so-called "eye of chaos"[21]. Regarding Fig. 4(i), the ATs appear wider, with colors along their boundaries suggesting period-doubling bifurcations. Secondary and tertiary structures are more pronounced and expansive compared to Fig. 4(g). Central holes within the ATs in Fig. 4(i) are more prominent than those in Fig. 4(h). To further visualize the forcing effects, we zoom into a specific region within each FPD to gain deeper insights into the system's dynamic behavior.

Figure 5(a) depicts a magnified region extracted from Fig. 4(g), providing a detailed view of the FPD. Within this FPD, the ATs are distinctly visible, each corresponding to oscillations characterized by a specific number of isospikes. Primary structures with 1, 2, 3, 4, and 5 isospikes are discernible, along with secondary structures featuring 3 and 5 isospikes,

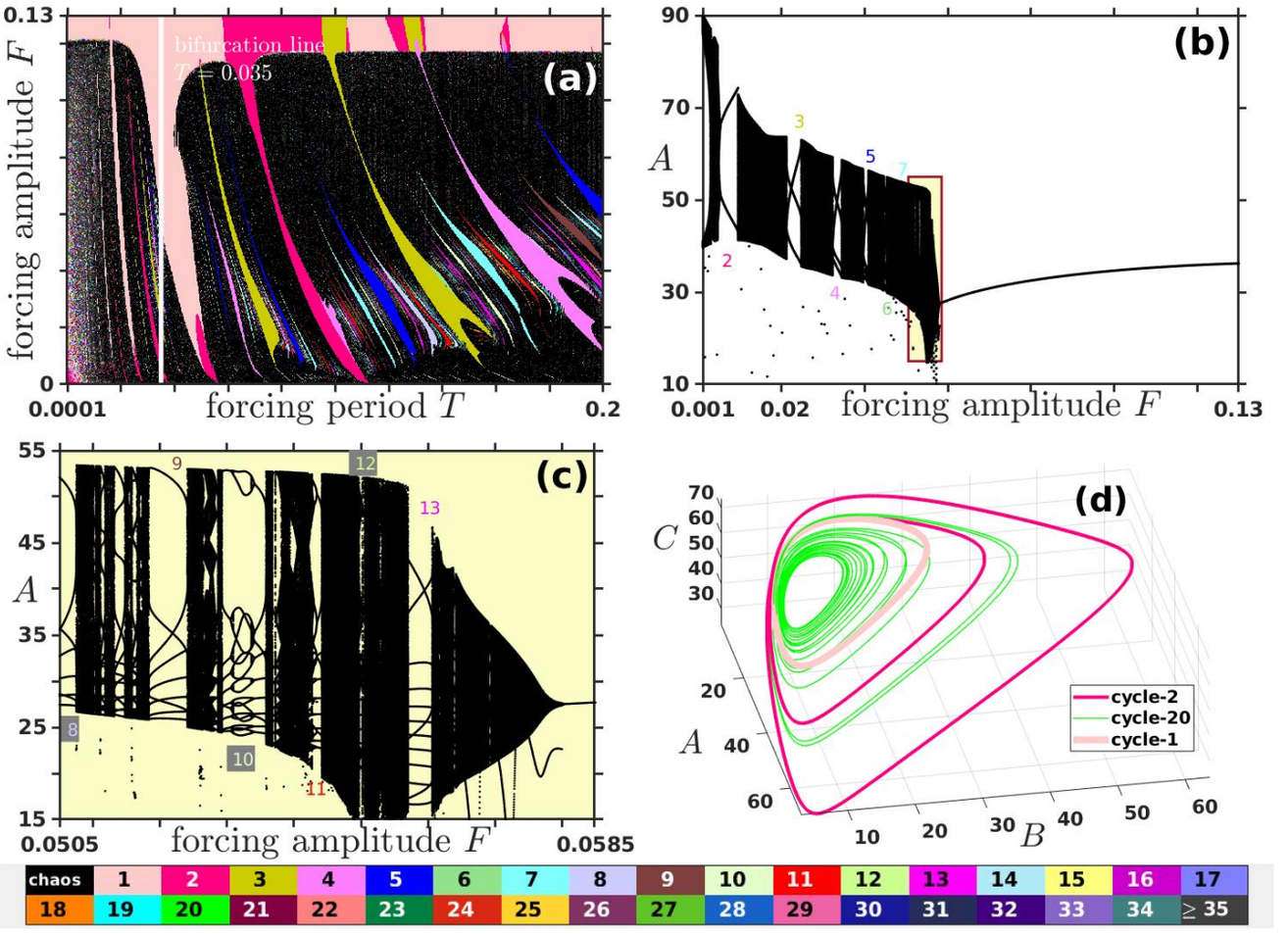

Figure 6. Analysis of the forcing regime at $P = 7.78$. (a) Forcing phase diagram F vs. T for the variable A, corresponding to the magnified rectangular region of Fig. 4(h). (b) Bifurcation diagram derived from the maxima of the time series along the line $T = 0.035$ depicted in (a). Noticeable are regions exhibiting regular behavior characterized by limit cycles-2 to 7. (c) Enlarged view of the highlighted yellow rectangular region from (b), enabling the distinction of regions featuring periodic behavior up to limit cycle-13. (d) Phase space representation illustrating various examples of limit cycles, including limit cycles-1 ($F = 0.13$) and 2 ($F = 0.006764$), along with an attractor displaying 20 isospikes ($F = 0.053168$) (refer to Table I for detailed descriptions of the aforementioned manifolds in phase space).

and tertiary structures comprising 4, 5, 7, 8, 10, 11, 13, and 14 isospikes. While higher-order structures (quaternary, quinary, etc.) may exist, they remain indistinguishable due to resolution limitations. To overcome the above mentioned hindrance, we highlight higher-order structures in the third column of Fig. 5 by showing an enlarged view of the sequence of the ATs. To close our analysis of Fig. 5(a), we notice that a tendency towards oscillations with fewer isospikes is visible for large amplitude forcing, with a separation between the predominant chaotic region and the periodic region with fewer isospikes.

We generated the BD depicted in Fig. 5(b) along the line $F = 0.117$ outlined in panel (a). This BD was built for 8192 values of the period forcing within the range $T \in [0.0001, 0.2]$ and reports the maxima of A. Abrupt peaks are observed, reminiscent of the concept of crises in dynamical systems. This is particularly notable for the case of limit cycles-1, where the size of the attractor can change dramatically. We selected nine points in the BD to illustrate their corresponding invariant manifolds in phase space: five limit cycles-1 presented in Fig. 5(c), and two limit cycles-2 and 3 displayed in Fig. 5(d). The sharp increase in the A value at points 2 and 3, along with the discontinuity between points 3 and 4, is evident in the phase space of Fig. 5(c), where the limit cycle corresponding to point 1 has a very small amplitude and appears as a point compared to the limit cycles corresponding to the other points. Conversely, the shape of the limit cycles remains consistent across most cases of limit cycles-1, except for those corresponding to points 1 and 2 at small T values. Similar phenomena were observed in prior studies[13]. Figure 5(d) showcases the limit cycles with two (points 5 and 6 in the BD) and three isospikes (points 7 and 8 in the BD), demonstrating that the size of the limit cycles depends on the period forcing T value, and the shape of the limit cycles differs from

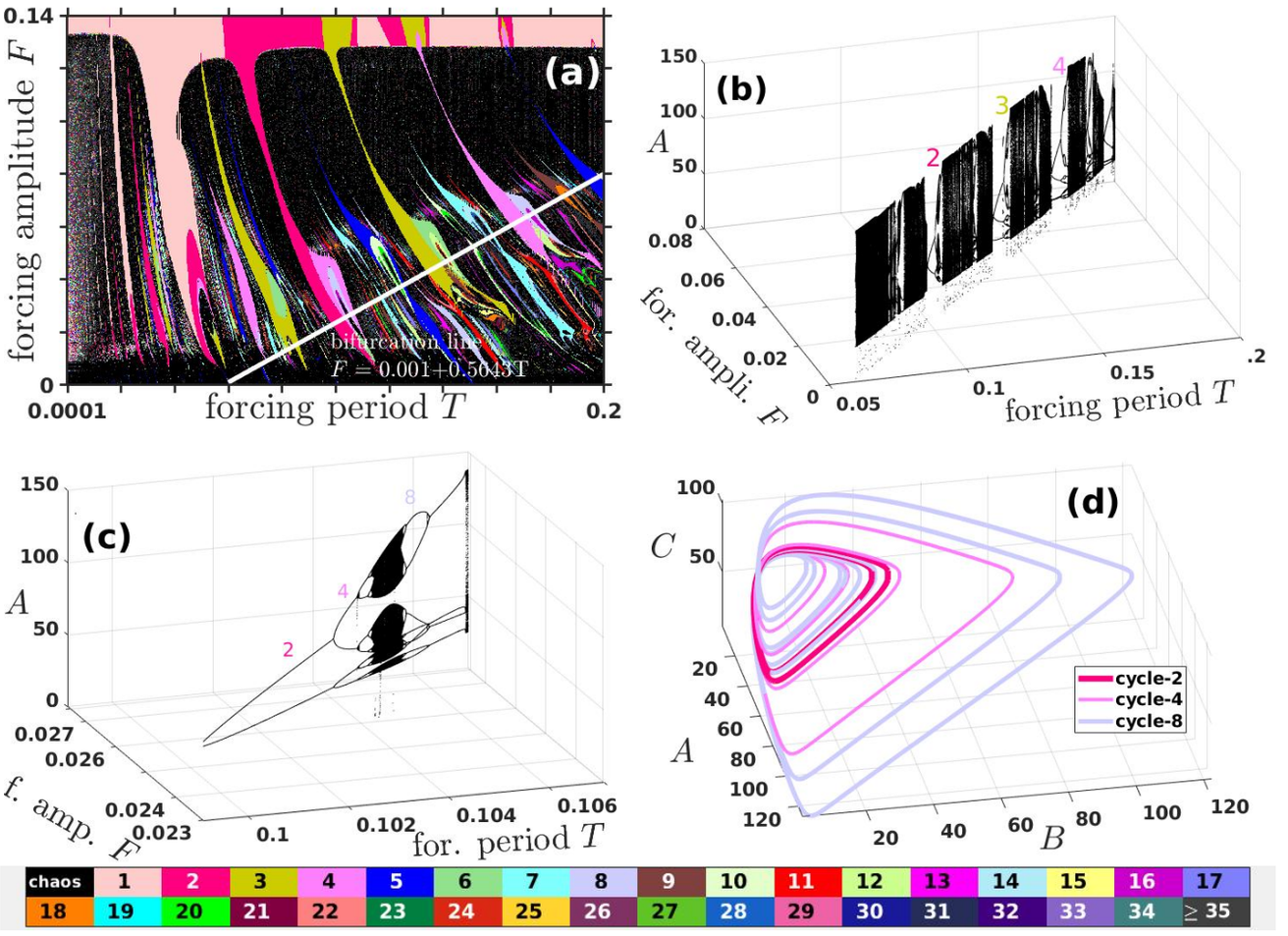

Figure 7. Analysis of the forcing when $P = 7.70$. (a) Forcing phase diagram F vs T for the variable A, corresponding to the magnified rectangular area in Fig. 4(i). (b) Bifurcation diagram derived from the maxima of the time series along the linear trajectory $F = 0.001 + 0.5013T$ depicted in (a). Regions demonstrating periodic behavior with limit cycles-2 to 4 are discernible. (c) An amplified view of the domain exhibiting a dominant limit cycle-2, revealing a period-doubling route to chaos. (d) Phase space illustrating various instances of limit cycles associated with the period-doubling bifurcation, each featuring 2, 4, and 8 isospikes obtained for $(T, F) = (0.099171, 0.023128)$ (limit cycle-2), $(T, F) = (0.103665, 0.025591)$ (limit cycle-4), and $(T, F) = (0.105619, 0.026823)$ (limit cycle-8) (refer to Table I for detailed information concerning the specified manifolds within the phase space).

most cases of limit cycles-1. Isospikes-adding, in analogy with period-adding observed when analyzing maps, becomes more evident in the magnification of the boxed region of the FPD shown in Fig. 5(e), where the primary, secondary, and some tertiary structures are distinguishable. The diagram of the number of isospikes in terms of the forcing period when the amplitude forcing is $F = 0.035$ is exhibited in Fig. 5(f), in which the AT's width is indicated and identified with the explicit number of isospikes with a subindex referring to the order of the periodic structure. Thus the three visible primary structures are represented by 1_1, 2_1 and 3_1, the secondary as 3_2 and 5_2, ..., until to 14_{13}, 15_9 and 15_{10}.

The selected region from Fig. 4(h) is presented in Fig. 6(a), revealing the same main features as observed in the FPD of Fig. 5(a), albeit with enlarged ATs displaying a proclivity towards a concave structure in their lower sections, eventually forming cavities situated in the central region of the ATs, as previously described. As a result of the enlargement of ATs, the discernment of third-order structures is possible within the sequence. This enlargement also enables the identification of chaotic behavior or the number of isospikes in ATs. The straight line $T = 0.005$ on the FPD corresponds to the BD depicted in Fig. 6(b), where interspersed regions of periodic and chaotic behavior are observable, quasiperiodicity is inferred in the boundaries of regular dynamics and chaotic windows. For elevated values of F, the dynamics in this region converge toward a limit cycle-1. However, identifying periodic windows with more than 6 isospikes becomes cumbersome. An amplified view of the BD within the demarcated region in Fig. 6(b) reveals additional regions of periodic behavior (see Fig. 6(c), where oscillatory domains with 17 isospikes are discernible). The presence of points below certain regions of the

Table I. Summary of phase space manifolds discussed in the article. All figures were generated using the parameters and initial conditions specified in Fig. 2, namely: $k_0 = 260$, $k_c = k_u = k_1 = 1$, $k_2 = 200$, $k_3 = 50$, and $(A_0, B_0, C_0) = (1, 1, 1)$.

P	T	F	**Manifold without forcing**	**Manifold with forcing**	**Manifold shown in**
7.83	-	-	limit cycle-1 (1 isospike)	-	Fig. 2(d)
	0.075	0.03		chaotic attractor	Fig. 4(d)
	0.001	0.117		limit cycle-1	Fig. 5(c)-1
	0.016743				Fig. 5(c)-2
	0.038943				Fig. 5(c)-3
	0.038973				Fig. 5(c)-4
	0.2				Fig. 5(c)-9
	0.066645			limit cycle-2	Fig. 5(d)-5
	0.08253				Fig. 5(d)-6
	0.0975			limit cycle-3	Fig. 5(d)-7
	0.13				Fig. 5(d)-8
7.78	-	-	limit cycle-4 (4 isospikes)	-	Fig. 2(e)
	0.075	0.03		limit cycle-8	Fig. 4(e)
	0.035	0.006764		limit cycle-2	Fig. 6(d)-2
		0.053168		limit cycle-20	Fig. 6(d)-20
		0.13		limit cycle-1	Fig. 6(d)-1
7.70	-	-	chaotic attractor	-	Fig. 2(f)
	0.075	0.03		limit cycle-3	Fig. 4(f)
	0.099171	0.023128		limit cycle-2	Fig. 7(d)-2
	0.103665	0.025591		limit cycle-4	Fig. 7(d)-4
	0.105619	0.026823		limit cycle-8	Fig. 7(d)-8

BDs may suggest the occurrence of boundary crises, as elaborated in[31,49]. For the purpose of illustrating the manifolds in phase space, Fig. 6(d) depicts the stable manifold obtained for 3 different values of the forcing amplitude F, showing the generation of limit cycle-2, ǫmplex oscillation with 20 isospikes, limit cycle-1. It is noteworthy to indicate that the choice of an oscillation with 20 isospikes is made deliberately because such an oscillation is located in a narrow window embedded in a predominantly chaotic region in the BD of Fig. 6(c) and with shorter amplitude oscillations compared to the those giving rise to low order limit cycles.

Figure 7(a) provides a magnified view of the selected rectangular region delineated in Fig. 4(i). The primary features of the FPD resemble those observed in previous examples; however, distinctive nuances are noteworthy: for low T values, in addition to the left segment of the primary AT, the sequence of regions delineating oscillations with increasing isospikes becomes more pronounced. Furthermore, the ATs, aside from being larger compared to previous cases, exhibit regions suggestive of period-doubling. The chaotic holes within the tongues persist even for secondary and tertiary structures. To discern diverse dynamical regimes within the FPD, we delineate the trajectory $F = 0.001 + 0.5013T$ within the intervals $T \in [0.06, 0.2]$ and $F \in [0.004, 0.08]$, and build the BD depicted in Fig. 7(b), where regions corresponding to the primary ATs are distinctly discernible. To emphasize the existence of period-doubling, we concentrate on the BD within the intervals $T \in [0.0991, 0.1071]$ and $F \in [0.0230064, 0.027578]$, encompassing the segment delineating the AT predominantly featuring two isospikes, as depicted in Fig. 7(c). Here, the period-doubling cascade route to chaos is evident, followed by a return to a periodic regime featuring 8 isospikes. Analogous to Figs. 6(b)–(c), some features are indicative of boundary interior crises that are observable, particularly at the terminus of the BDs in Figs. 7(b)–(c). Finally, Fig. 7(d) portrays three limit cycles extracted from the BD in Fig. 7(c). A summary of phase space manifolds discussed above is given in Table I.

Based on the results obtained from the analysis of forcing in the three examined cases (Figs. 4–7), we observe that periodic forcing applied to the system exhibiting a limit cycle-1 primarily induces chaotic behavior for F values below a threshold associated with strong coupling, leading to periodic behavior resembling the forcing signal across all cases. Conversely, when the forcing is applied to the system with complex limit cycles, chaotic behavior remains predominant, albeit with larger ATs. Arnold's tongues exhibit further enlargement when the forcing is applied to a chaotic regime. Consequently, these observations suggest the manifestation of phenomena such as chaos control[6] and chaotification[69].

Another observation can be made when looking at the effect of periodic forcing on limit cycle-4 and chaotic attractors (Figs. 4(h) and (i)). In the first row of Fig. 8, magnified regions of Fig. 4(h) (Fig. 8(a)) and Fig. 4(i) (Fig. 8(b)) are shown. Figure 8(a) shows the "chaotic holes," which correspond to specified primary ATs with, in this case, 6 and 7 isospikes as the main periodicity. The AT-like structure exhibits a kind of "hole" with predominant chaotic behavior emerging, but inside, there are some structures whose numbers of isospikes correspond to 24 and 30 for the case of the AT with 6 isospikes, and 28 and 35 for the AT with 7 isospikes. Figure 8(b) further shows the "eye of chaos" in the primary AT featured by 3 isospikes as its main periodicity. We also observe that secondary structures display the "eyes of chaos" and tertiary structures exhibit diverse shapes reminiscent of the so-called "shrimps" and "ring structures." Moreover, inside the

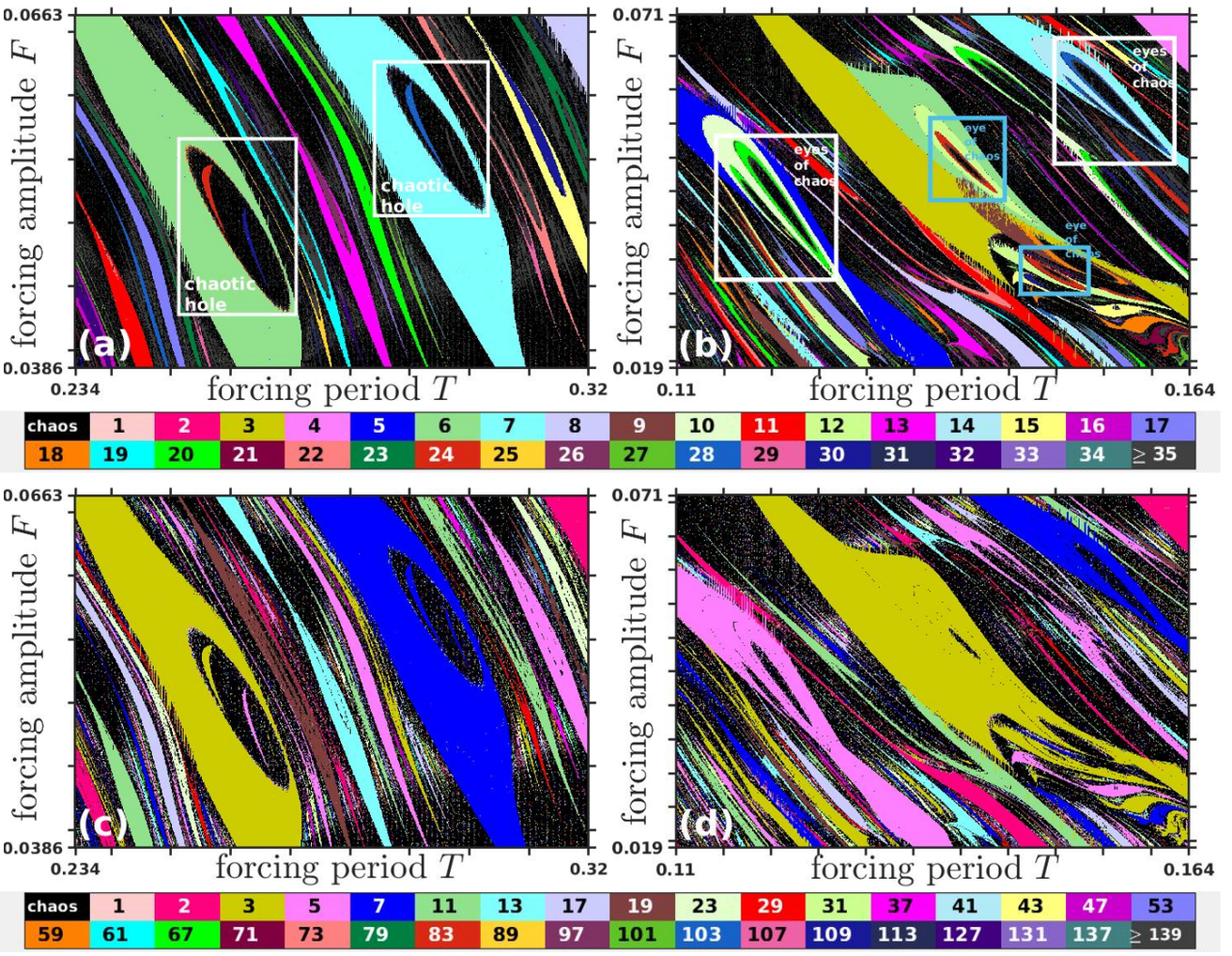

Figure 8. Magnified views of forcing phase diagrams (FPD) showing interesting dynamical structures (a) and (c) when $P = 7.78$ where the region of "chaos holes" are distinguished in the primary Arnold's tongues (ATs)-like structures with 6 and 7 isospikes. (b) and (d) when $P = 7.70$ where the "eye(s) of chaos" structures are identified in the secondary AT-like structures with the main number of isospikes of 5 and 7. Note that ring structures are present inside the "eye(s) of chaos" and also found in some of the tertiary AT-like structures. Figures in the first row are featured by the color bar indicating the number of isospikes of the oscillations. As the number of isospikes per cycle might be greater than 35, we alternatively characterize the figures in the second row using a color code based on the higher prime number factor, which allows us to notice the presence of additional higher-order and also the period-doubling bifurcation scenario in most of those structures.

"eye(s) of chaos" are also present the "ring structures." As stated in the FPD from Figs. 5(e) and especially in the diagram of Fig. 1(f), there are number of high-order structures whose number of isospikes are greater than 34 that is the limit of clear visualization of the number of isospikes according to the color code shown in Figs. 3–7 and under the first row of Fig. 8. To extend the detection of higher–order structures, we introduce a color code based on the maximum prime factor of the number of isospikes as in[58], where each color represents the maximum prime factor of the number of isospikes. For instance, the color representing an oscillation with 91 isospikes is 13, as 13 is the maximum prime factor of 91 (7 and 13). This color can also represent 26, 39, 52, 65, 78, 104, 117, 130, 143, 156, 169, 182, 195, 208, 221, and so forth. Prime factors larger than 139 are represented in dark gray. This convention ensures that each color represents the multiples of each prime number from 2 to 139. Chaos is depicted in black in this color code. In the second row of Fig. 8, we use the above-mentioned color code for a new representation of Figs. 8(a)–(b).

With the aim of obtaining a global overview of the forcing effects on the system, we generated a sequence of PPs to see how the dynamical landscapes change due to the forcing (Fig. 9), Figure 9(a) is the same PP shown in Fig. 3(b) but in terms of the new color code. It describes the unforced situation. We start by fixing the forcing period $T = 0.15$ and varying the amplitude forcing F. For a quite small amplitude

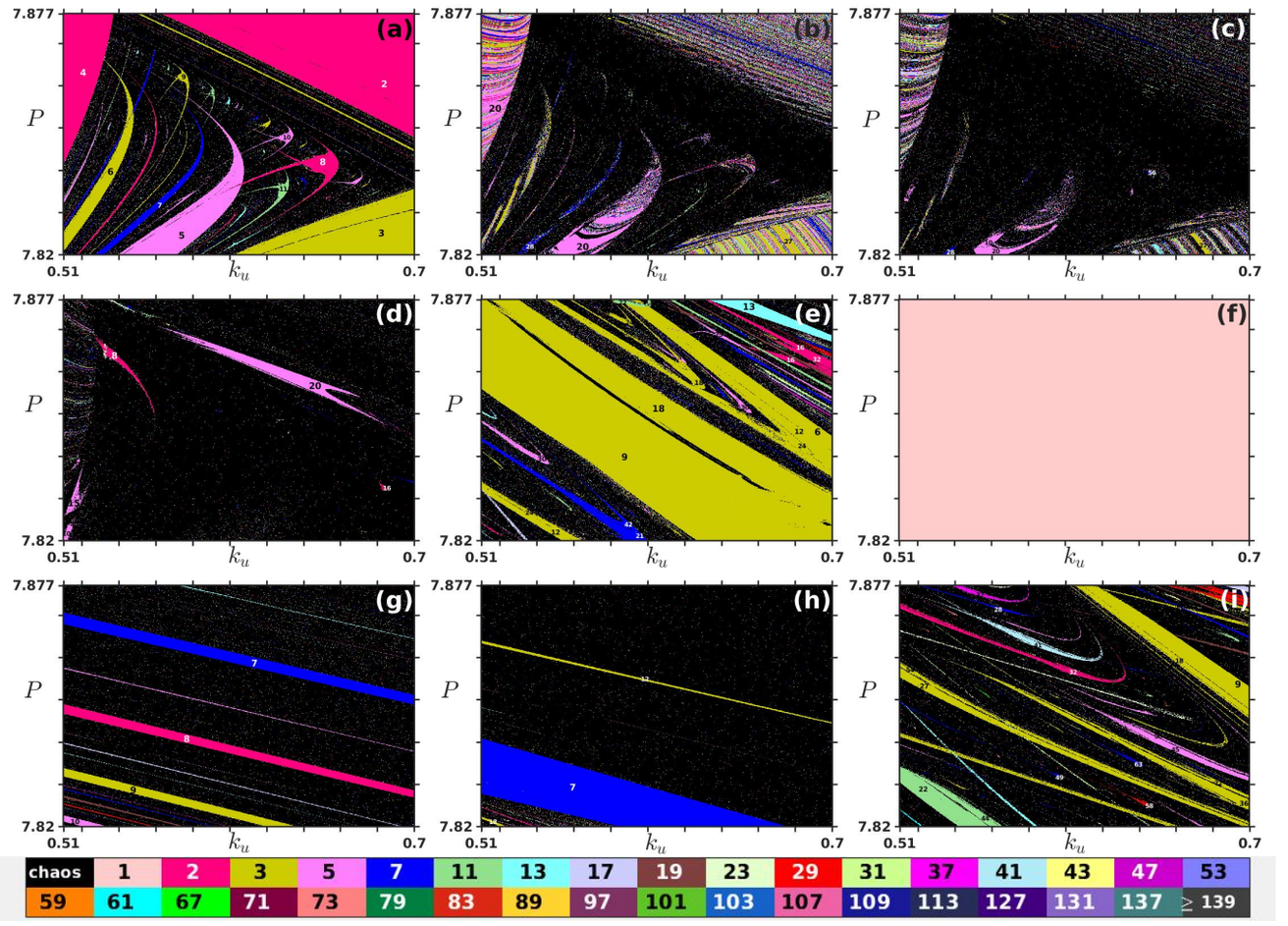

Figure 9. Changing the landscape of the parameter planes by forcing. Parameter planes P vs. k_u corresponding to Fig. 3(b) represented in terms of the color code based on the maximum prime factor of the number of isospikes as in Figs. 8(c)–(d). The used representation allows us to distinguish oscillations with large numbers of isospikes. (a) No forcing. Forcing cases with (b) $T = 0.15$ and $F = 0.000025$, (c) $T = 0.15$ and $F = 0.00025$, (d) $T = 0.15$ and $F = 0.0025$, (e) $T = 0.15$ and $F = 0.025$, (f) $T = 0.15$ and $F = 0.25$, (g) $T = 0.05$ and $F = 0.045$, (h) $T = 0.1$ and $F = 0.045$, (i) $T = 0.2$ and $F = 0.045$.

$F = 0.000025$, the changes in the PP (Fig. 9(b)). Most of the structures of the unforced PP are preserved, albeit with changes in the dynamic that they represent, notably by the increasing number of isospikes and the pervading chaotic regions. By increasing the forcing tenfold ($F = 0.00025$), the PP exhibits more changes with a more important tendency of chaos (Fig. 9(c)). By another tenfold increase in the forcing ($F = 0.0025$), chaos is largely predominant, and only some vestiges keep the original PP. A further tenfold increase of the forcing ($F = 0.025$) enhances the periodic behavior that becomes dominant in the PP (Fig. 9(e)). Another increase by tenfold ($F = 0.25$) implies an intensive forcing that drives the system to a regular periodic behavior with the same period as the forcing signal for all the situations (Fig. 9(f)). Maintaining fixed the forcing to $F = 0.045$ and varying the period also induce changes in the PP; thus, when $T = 0.05$, the original landscape of the PP has totally changed, and the main visible feature is a sequence of lines going diagonally from the bottom left part indicating periodic behavior with 10, 9, 8, and 7 isospikes (Fig. 9(g)). When $T = 0.1$, there is a wide region displaying a periodic behavior with 7 isospikes and two thin lines related to 12 and 18 isospikes (Fig. 9(h)). Finally, when $T = 0.2$, the landscape is completely different from that of the unforced PP, with the emergence of new regions characterized by a large number of isospikes (Fig. 9(i)). To complement the observations mentioned above, Fig. 10 shows example attractors obtained when a periodic forcing is applied for various periods (columns) and amplitudes (rows). As a reference, the gray trajectory corresponds to the chaotic attractor obtained without forcing. This figure illustrates abrupt changes in the attractor in terms of nature and size that can occur when the period or amplitude is modified, consistent with an abrupt change of the landscape shown in Fig. 9.

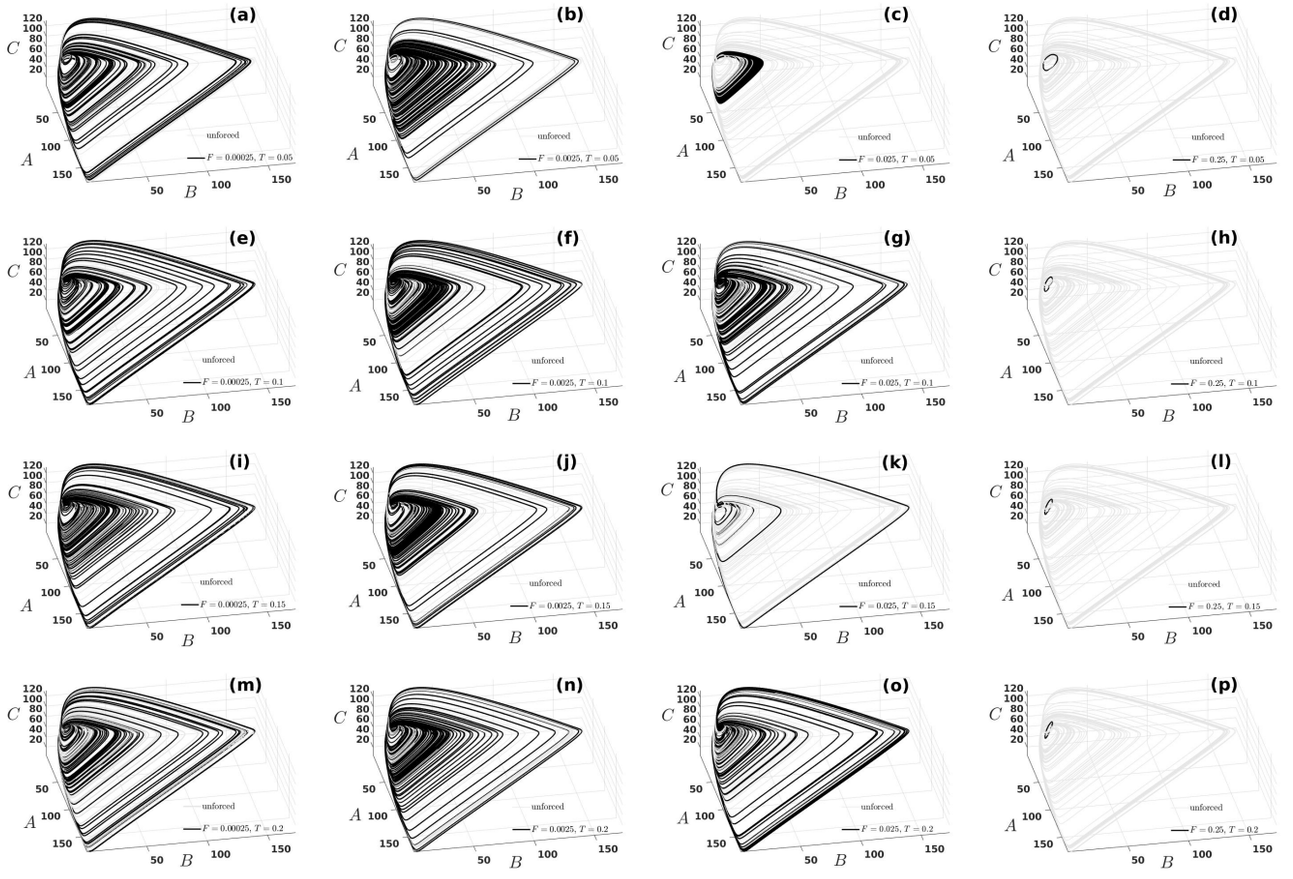

Figure 10. Effects of the period and amplitude forcing on the shape of attractors. The parameter values are $k_0 = 260$, $k_c = k_u = k_1 = 1$, $k_2 = 200$, $k_3 = 50$, $k_u = 0.6$ and $P = 7.845$. **First row:** $T = 0.05$ (a) $F = 0.00025$, (b) $F = 0.0025$, (c) $F = 0.025$ and (d) $F = 0.25$. **Second row:** $T = 0.10$ (e) $F = 0.00025$, (f) $F = 0.0025$, (g) $F = 0.025$ and (h) $F = 0.25$. **Third row:** $T = 0.15$ (i) $F = 0.00025$, (j) $F = 0.0025$, (k) $F = 0.025$ and (l) $F = 0.25$. **Fourth row:** $T = 0.20$ (m) $F = 0.00025$, (n) $F = 0.0025$, (o) $F = 0.025$ and (p) $F = 0.25$. Note that the gray and black attractors correspond to the unforced and forced cases, respectively.

IV. CONCLUSIONS AND PERSPECTIVES

Our analysis of the autocatalator provides an exhaustive overview of the dynamic behavior of this system, both in unforced and forced cases. The use of the isospikes and LLEs allowed us to identify the scarce chaotic regions in the system. Those chaotic regions exhibit interesting dynamic features, such as the presence of shrimp sequences going towards accumulation points and the period-doubling route to chaos. The sinusoidal forcing gives rise to a myriad of possibilities to change the dynamic behavior of the system, as shown in the forcing phase diagrams (period vs amplitude). We exemplified the forcing effects with three specific transitions: limit cycle $\rightarrow$ chaos, limit cycle $\rightarrow$ higher order limit cycle, and chaos $\rightarrow$ limit cycle. In all cases, we observed an increase in the number of isospikes with the period. On the contrary, when the forcing amplitude increases above a certain threshold, the entrained signal adopts a regular limit cycle with the same period as the forcing, regardless of the forcing period. In most cases, the contour shapes of unforced and forced attractors are similar, even though the sizes might be quite different.

In the forcing phase diagram, the abundance and diversity of the entrained regions are more evident when the original signal is more complex; thus, an original chaotic signal can give rise to a forcing phase diagram with much more dynamic richness than a limit cycle.

Finally, we observed the changes experienced in the PP when forcing acts with different amplitudes and periods. For a fixed forcing period, the increase in the forcing amplitude destroys the structures of regular behavior, even for small values of the amplitude forcing, for which chaos becomes predominant. Intermediate values of the amplitude forcing favor the apparition of large regions of periodic behavior. When the forcing amplitude is sufficiently high, simple oscillation with a limit cycle-1 is obtained regardless of the parameter values. On the other hand, when keeping the forcing amplitude constant to an intermediate value, increasing the forcing period gives rise to a region of complex oscillations in the PP characterized by a large number of isospikes per oscillation cycle

and probably to quasiperiodic behavior.

As perspectives of this work, it will be interesting to study other models, especially in biological contexts, and to apply different types of forcing, as those pulsatile used in radiotherapy treatments[60], or quasiperiodic[10,23]. Other interesting aspects, such as the multistability, the existence of crises, and the emergence of extreme events, may also deserve special attention in further works.

ACKNOWLEDGMENTS

GMRA and TK have been supported by the National Science Centre, Poland, OPUS Programs (Projects No. 2018/29/B/ST8/00457 and 2021/43/B/ST8/00641). This project has received funding from the European Union's Horizon 2020 research and innovation programme under the Marie Sklodowska-Curie grant agreement No 101034383. Computational resources have been provided by the Consortium des Équipements de Calcul Intensif (CÉCI), funded by the Fonds de la Recherche Scientifique de Belgique (F.R.S.-FNRS) under Grant No. 2.5020.11 and by the Walloon Region.

AUTHOR DECLARATIONS

Conflict of Interest

The authors have no conflicts to disclose.

Author Contributions

G. M. Ramírez-Ávila: Conceptualization (equal); Formal analysis (equal); Investigation (equal); Methodology (equal); Software (lead); Validation (equal); Visualization (equal); Writing — review & editing (equal). **T. Kapitaniak:** Conceptualization (equal); Formal analysis (equal); Investigation (equal); Methodology (equal); Validation (equal); Visualization (equal); Writing — review & editing (equal); Resources (lead). **D. Gonze:** Conceptualization (equal); Formal analysis (equal); Investigation (equal); Methodology (equal); Validation (equal); Visualization (equal); Writing — review & editing (equal).

DATA AVAILABILITY

The data that support the findings of this study are available from the corresponding author upon reasonable request.

REFERENCES

[1] Aihara, K., Takabe, T., and Toyoda, M., "Chaotic neural networks," Phys. Lett. A **144**, 333–340 (1990).
[2] Almeida, S., Chaves, M., and Delaunay, F., "Transcription-based circadian mechanism controls the duration of molecular clock states in response to signaling inputs," J. Theor. Biol. **484**, 110015 (2020).
[3] Araújo, N. S., Reyes-Garcia, S. Z., Brogin, J. A. F., Bueno, D. D., Cavalheiro, E. A., Scorza, C. A., and Faber, J., "Chaotic and stochastic dynamics of epileptiform-like activities in sclerotic hippocampus resected from patients with pharmacoresistant epilepsy," PLoS Comput. Biol. **18**, 1–31 (2022).
[4] Babloyantz, A., Salazar, J. M., and Nicolis, C., "Evidence of chaotic dynamics of brain activity during the sleep cycle," Phys. Lett. A **111**, 152–156 (1985).
[5] Baptista, M. S.and Caldas, I. L., "Phase-locking and bifurcations of the sinusoidally-driven double scroll circuit," Nonlinear Dyn. **17**, 119–139 (1998).
[6] Boccaletti, S., Grebogi, C., Lai, Y. C., Mancini, H., and Maza, D., "The control of chaos: theory and applications," Phys. Rep. **329**, 103–197 (2000).
[7] Chialvo, D. R., Gilmour Jr, R. F., and Jalife, J., "Low dimensional chaos in cardiac tissue," Nature **343**, 653–657 (1990).
[8] Choe, C.-U., Höhne, K., Benner, H., and Kivshar, Y. S., "Chaos suppression in the parametrically driven Lorenz system," Phys. Rev. E **72**, 036206 (2005).
[9] Decroly, O.and Goldbeter, A., "Birhythmicity, chaos, and other patterns of temporal self-organization in a multiply regulated biochemical system," P. Natl. Acad. Sci. USA **79**, 6917–6921 (1982).
[10] Ding, M., Grebogi, C., and Ott, E., "Evolution of attractors in quasiperiodically forced systems: From quasiperiodic to strange nonchaotic to chaotic," Phys. Rev. A **39**, 2593–2598 (1989).
[11] Faure, P.and Korn, H., "Is there chaos in the brain? i. concepts of nonlinear dynamics and methods of investigation," C. R. Acad. Sci. Paris, Ser. III **324**, 773–793 (2001).
[12] Field, R. J., Freire, J. G., and Gallas, J. A. C., "Quint points lattice in a driven Belousov–Zhabotinsky reaction model," Chaos **31**, 053124 (2021).
[13] Fouodji Tsotsop, M., Kengne, J., Kenne, G., and Tabekoueng Njitacke, Z., "Coexistence of multiple points, limit cycles, and strange attractors in a simple autonomous hyperjerk circuit with hyperbolic sine function," Complexity **2020**, 6182183 (2020).
[14] Franz, M.and Zhang, M., "Suppression and creation of chaos in a periodically forced Lorenz system," Phys. Rev. E **52**, 3558–3565 (1995).
[15] Freire, J. G., Calderón-Cárdenas, A., Varela, H., and Gallas, J. A. C., "Phase diagrams and dynamical evolution of the triple-pathway electro-oxidation of formic acid on platinum," Phys. Chem. Chem. Phys. **22**, 1078–1091 (2020).
[16] Freire, J. G., Field, R. J., and Gallas, J. A. C., "Relative abundance and structure of chaotic behavior: The nonpolynomial Belousov–Zhabotinsky reaction kinetics," J. Chem. Phys. **131**, 044105–8 (2009).
[17] Freire, J. G.and Gallas, J. A. C., "Stern-Brocot trees in the periodicity of mixed-mode oscillations," Phys. Chem. Chem. Phys. **13**, 12191–12198 (2011).
[18] Freire, J. G., Gallas, M. R., and Gallas, J. A. C., "Stability mosaics in a forced Brusselator," Eur. Phys. J.-Spec. Top. **226**, 1987–1995 (2017).
[19] Gallas, J. A. C., "Dissecting shrimps: results for some one-dimensional physical models," Physica A **202**, 196–223 (1994).
[20] Gallas, J. A. C., "Chirality observed in a driven ruthenium-catalyzed Belousov–Zhabotinsky reaction model," Phys. Chem. Chem. Phys. **23**, 25720–25726 (2021).
[21] Gallas, J. A. C., "Non-quantum chirality in a driven Brusselator," J. Phys.-Condens. Mat. **34**, 144002 (2022).
[22] Gallas, M. R.and Gallas, J. A. C., "Nested arithmetic progressions of oscillatory phases in Olsen's enzyme reaction model," Chaos **25**, 064603 (2015).
[23] Gentile, G., Mazzoccoli, A., and Vaia, F., "Forced quasi-periodic oscillations in strongly dissipative systems of any finite dimension," Commun. Contemp. Math. **21**, 1850064 (2019).
[24] Glass, L.and Mackey, M. C., *From Clocks to Chaos. The Rhythms of Life* (Princeton University Press, Princeton, 1988).
[25] Glass, L.and Malta, C. P., "Chaos in multi-looped negative feedback systems," J. Theor. Biol. **145**, 217–223 (1990).
[26] Glossop, N. R. J., Lyons, L. C., and Hardin, P. E., "Interlocked feedback loops within the *Drosophila* circadian oscillator," Science **286**, 766–768 (1999).

[27]Goldbeter, A., Gonze, D., Houart, G., Leloup, J.-C., Halloy, J., and Dupont, G., "From simple to complex oscillatory behavior in metabolic and genetic control networks," Chaos **11**, 247–260 (2001).
[28]Goldbeter, A.and Leloup, J.-C., "From circadian clock mechanism to sleep disorders and jet lag: Insights from a computational approach," Biochem. Pharmacol. **191**, 114482 (2021).
[29]Gonze, D.and Goldbeter, A., "Entrainment versus chaos in a model for a circadian oscillator driven by light-dark cycles," J. Stat. Phys. **101**, 649–663 (2000).
[30]Gonze, D., Markadieu, N., and Goldbeter, A., "Selection of in-phase or out-of-phase synchronization in a model based on global coupling of cells undergoing metabolic oscillations," Chaos **18**, 037127–12 (2008).
[31]Grebogi, C., Ott, E., and Yorke, J. A., "Crises, sudden changes in chaotic attractors, and transient chaos," Physica D **7**, 181–200 (1983).
[32]Gérard, C.and Goldbeter, A., "From simple to complex patterns of oscillatory behavior in a model for the mammalian cell cycle containing multiple oscillatory circuits," Chaos **20**, 045109 (2010).
[33]Heltberg, M. L., Krishna, S., and Jensen, M. H., "On chaotic dynamics in transcription factors and the associated effects in differential gene regulation," Nature Comm. **10**, 71 (2019).
[34]Heltberg, M. L., Krishna, S., Kadanoff, L. P., and Jensen, M. H., "A tale of two rhythms: Locked clocks and chaos in biology," Cell Syst. **12**, 291–303 (2021).
[35]Hordijk, W.and Steel, M., "Autocatalytic networks at the basis of life's origin and organization," Life **8**, 62 (2018).
[36]Ivanović-Šašić, A. Z., Marković, V. M., Anić, S. R., Kolar-Anić, L. Z., and Čupić, Z. D., "Structures of chaos in open reaction systems," Phys. Chem. Chem. Phys. **13**, 20162–20171 (2011).
[37]Jensen, M. H.and Krishna, S., "Inducing phase-locking and chaos in cellular oscillators by modulating the driving stimuli," FEBS Lett. **586**, 1664–1668 (2012).
[38]Jiménez, A., Lu, Y., Jambhekar, A., and Lahav, G., "Principles, mechanisms and functions of entrainment in biological oscillators," Interface Focus **12**, 20210088 (2022).
[39]Kalishin, E. Y., Goncharenko, M. M., Khavrus, V. A., and Strizhak, P. E., "Periodic, mixed-mode, and chaotic regimes in the Belousov-Zhabotinskii reaction catalyzed by ferroin," Kinet. Catal+. **43**, 233–244 (2002).
[40]Karavaev, A. S., Ishbulatov, Y. M., Ponomarenko, V. I., Bezruchko, B. P., Kiselev, A. R., and Prokhorov, M. D., "Autonomic control is a source of dynamical chaos in the cardiovascular system," Chaos **29**, 121101 (2019).
[41]Kawczyński, A. L., Khavrus, V. O., and Strizhak, P. E., "Complex mixed-mode periodic and chaotic oscillations in a simple three-variable model of nonlinear system," Chaos **10**, 299–310 (2000).
[42]Korn, H.and Faure, P., "Is there chaos in the brain? ii. experimental evidence and related models," C. R. Biologies **326**, 787–840 (2003).
[43]Lai, Q., Zhao, X.-W., Huang, J.-N., Pham, V.-T., and Rajagopal, K., "Monostability, bistability, periodicity and chaos in gene regulatory network," Eur. Phys. J.-Spec. Top. **227**, 719–730 (2018).
[44]Leloup, J.-C.and Goldbeter, A., "Chaos and birhythmicity in a model for circadian oscillations of the per and tim proteins in drosophila," J. Theor. Biol. **198**, 445–459 (1999).
[45]Leloup, J.-C., Gonze, D., and Goldbeter, A., "Limit cycle models for circadian rhythms based on transcriptional regulation in drosophila and neurospora," J. Biol. Rhythm. **14**, 433–448 (1999).
[46]Li, Z., Bianco, S., Zhang, Z., and Tang, C., "Generic properties of random gene regulatory networks," Quant. Biol. **1**, 253–260 (2013).
[47]Mathias, A. C.and Rech, P. C., "Changes in the dynamics of a Rössler oscillator by an external forcing," Chinese Phys. Lett. **30**, 030502 (2013).
[48]Nielsen, K., Sørensen, P. G., and Hynne, F., "Chaos in glycolysis," J. Theor. Biol. **186**, 303–306 (1997).
[49]de Oliveira, J. A., de Mendonça, H. M. J., Favarim, V. A., de Carvalho, R. E., and Leonel, E. D., "Boundary crises and supertrack orbits in the Gauss map," Eur. Phys. J.-Spec. Top. **231**, 381–384 (2022).
[50]Olsen, L. F., "Complex dynamics in an unexplored simple model of the peroxidase–oxidase reaction," Chaos **33**, 023102 (2023).
[51]Olsen, L. F.and Degn, H., "Chaos in an enzyme reaction," Nature **267**, 177–178 (1977).
[52]Olsen, L. F.and Lunding, A., "Chaos in the peroxidase–oxidase oscillator," Chaos **31**, 013119 (2021).
[53]Peng, B., Scott, S. K., and Showalter, K., "Period doubling and chaos in a three-variable autocatalator," J. Phys. Chem. **94**, 5243–5246 (1990).
[54]Petrov, V., Scott, S. K., and Showalter, K., "Mixed-mode oscillations in chemical systems," J. Chem. Phys. **97**, 6191–6198 (1992).
[55]Pyragas, K., "Delayed feedback control of chaos," Philos. T. R. Soc. A **364**, 2309–2334 (2006).
[56]Qu, Z., "Chaos in the genesis and maintenance of cardiac arrhythmias," Prog. Biophys. Mol. Bio. **105**, 247–257 (2011).
[57]Rachwalska, M.and Kawczyński, A. L., "New types of mixed-mode periodic oscillations in the Belousov-Zhabotinsky reaction in continuously ttirred tank teactors," J. Phys. Chem. A **103**, 3455–3457 (1999).
[58]Ramírez-Ávila, G. M., Depickère, S., Jánosi, I. M., and Gallas, J. A. C., "Distribution of spiking and bursting in Rulkov's neuron model," Eur. Phys. J.-Spec. Top. **231**, 319–328 (2022).
[59]Ramírez-Ávila, G. M., Kurths, J., and Gallas, J. A. C., "Ubiquity of ring structures in the control space of complex oscillators," Chaos **31**, 101102 (2021).
[60]Ramírez-Ávila, G. M., Kurths, J., Gonze, D., and Dupont, G., "Exploring chronomodulated radiotherapy strategies in a chaotic population model," Chaos Soliton. Fract. **173**, 113743 (2023).
[61]Rashid, M. M.and Kurata, H., "Coupling protocol of interlocked feedback oscillators in circadian clocks," J. R. Soc. Interface **17**, 20200287 (2020).
[62]Romond, P.-C., Rustici, M., Gonze, D., and Goldbeter, A., "Alternating oscillations and chaos in a model of two coupled biochemical oscillators driving successive phases of the cell cycle," Ann. NY Acad. Sci. **879**, 180–193 (1999).
[63]Schmitz, R. A., Graziani, K. R., and Hudson, J. L., "Experimental evidence of chaotic states in the Belousov–Zhabotinskii reaction," J. Chem. Phys. **67**, 3040–3044 (1977).
[64]van Soest, I., del Olmo, M., Schmal, C., and Herzel, H., "Nonlinear phenomena in models of the circadian clock," J. R. Soc. Interface **17**, 20200556 (2020).
[65]Stone, E. F., "Frequency entrainment of a phase coherent attractor," Phys. Lett. A **163**, 367–374 (1992).
[66]Werner, J., Pietsch, T., Hilker, F., and Arndt, H., "Intrinsic nonlinear dynamics drive single-species systems," P. Natl. Acad. Sci. USA **119**, e2209601119 (2022).
[67]Wolf, A., Swift, J. B., Swinney, H. L., and Vastano, J. A., "Determining lyapunov exponents from a time series," Physica D **16**, 285–317 (1985).
[68]Wulff, K., Porcheret, K., Cussans, E., and Foster, R., "Sleep and circadian rhythm disturbances: multiple genes and multiple phenotypes," Current Opinion in Genetics Development **19**, 237–246 (2009).
[69]Zhang, H., Liu, D., and Wang, Z., *Controlling chaos: suppression, synchronization and chaotification* (Springer London, 2009).
[70]Zhang, Z., Ye, W., Qian, Y., Zheng, Z., Huang, X., and Hu, G., "Chaotic motifs in gene regulatory networks," PloS one **7**, e39355 (2012).
[71]Zhao, J., Chen, Y., and Wang, J., "Transient complex oscillations in a closed chemical system with coupled autocatalysis," J. Chem. Phys. **122**, 114514 (2005).